Jurnal Pijar MIPA
https://jurnalfkip.unram.ac.id/index.php/JPM
ISSN 1907-1744 (Print)
ISSN 2460-1500 (Online)

The Effect of Polyetherimide Polymer Membrane Composition on the Performance Efficiency of Dye Sensitized Solar Cell (DSSC) Based on Natural Photosensitizer of Butterfly Pea Flowers

Fadlurachman Faizal Fachrirakarsie, Nita Kusumawati*

Department of Chemistry, Universitas Negeri Surabaya, Surabaya, Indonesia
*E-mail: nitakusumawati@unesa.ac.id

Received: March 9, 2024. Accepted: May 13, 2024. Published: May 25, 2024

Abstract: Global energy consumption will grow 1.3% in 2023-2024. This raises concerns about the scarcity of energy sources, most of which come from coal. This research is a true experiment with a one-shot case study design and aims to analyze the Dye-Sensitized Solar Cell (DSSC) from butterfly pea flowers (BPF) extract. However, DSSC has significant problems with liquid electrolyte leakage and solvent evaporation. Therefore, polyetherimide (PEI) membranes were investigated to overcome this problem. The BPF extract was examined for wavelengths, producing 573 nm and 617 nm wavelengths. The band gap was also checked, and it was found to produce 0.52 eV. The membrane used has five variations, where M_3 is the most stable, with a reduction in performance efficiency of only 98%. The membrane has a porous surface, asymmetric structure, and a crystallinity degree of 12.77%. Overall, this membrane shows the most optimal performance in DSSC among other membranes.

Keywords: Butterfly Pea Flowers; Efficiency; Energy; DSSC; Polyetherimide.

Introduction

Global energy consumption grew by 1.3% in 2023-2024 and is expected to increase in the future [1,2,3]. The emergence of the industrial revolution and a significant increase in human population have triggered excessive energy exploitation of global fossil fuel resources [4]. This raises many concerns because fossil fuels are increasingly depleting, and combustion impacts the environment [5]. To answer this problem, solar cells are the best choice because of the abundance of sources that do not cause environmental pollution. This cell is a sophisticated technology that converts solar energy into electrical energy. The cells generally utilize silicon to absorb photons emitted by sunlight [6]. However, high production costs and environmental problems arising from silicon's toxicity and non-biodegradable nature have limited its widespread utilization [7].

Dye-sensitized solar cells (DSSC) emerged to replace silicon-based solar cells. DSSC is a solar cell that uses TiO_2 as a working electrodes. DSSC utilizes TiO_2 to transfer electrons from the photosensitizer, which has absorbed photons and converted them to electrical energy. DSSC is a promising solution to future energy problems because its materials and structures are more straightforward than silicon-based solar cells [8,9]. Besides that, the most widely used photosensitizer is a ruthenium complex compound. These photosensitizers are challenging to synthesize and expensive [10]. As a solution, natural photosensitizers emerge from several plant pigments, including butterfly pea flower (BPF) anthocyanin, spinach leaf chlorophyll, and turmeric curcumin. The anthocyanins have a more comprehensive color range due to the influence of pH, so they greatly influence the efficiency of DSSC performance. This pigment undergoes excitation and charge transfer with the TiO_2 photoanode. This photoanode generally comprises nanoparticles with a large contact surface, thereby increasing the ability of light absorption by anthocyanins [11].

Electrolytes are another essential part of DSSC. The electrolyte is responsible for transporting charge from the photocathode to the photoanode. Liquid electrolytes with the I^-/I_3^- redox couple are known to have the highest performance efficiency [12]. Nevertheless, liquid electrolyte leakage and solvent evaporation limit their use over a long period. As a solution, polymer membranes emerged with the advantages of high ionic conductivity and flexible production scales. This technology uses polymers as a matrix that retains liquid electrolytes. Therefore, polymer membranes can overcome the weaknesses of liquid electrolytes [13]. Polyetherimide (PEI) is a polymer membrane with excellent chemical stability and thermal resistance reaching 500 °C. This polymer membrane has a higher porosity and smaller pore size than other superior polymers, such as polysulfone (PSf) and polyvinylidene fluoride (PVDF). This properties has the potential to prevent liquid electrolyte leakage.

In this research, the PEI polymer membrane was printed using knife casting. Dimethylacetamide (DMAc) solvent was used to obtain a homogeneous membrane structure. The relative energy difference (RED) between the PEI polymer membrane and DMAc solvent is 0.94 (RED < 1), undertaking perfect solubility with the formation of tiny pores and high porosity in the membrane [14,15]. The composition of PEI/DMAc was varied to obtain an optimal membrane with high porosity and a small enough pore size

How to Cite:
Fachrirakarsie, F. F., & Kusumawati, N. (2024). The Effect of Polyetherimide Polymer Membrane Composition on the Performance Efficiency of Dye Sensitized Solar Cell (DSSC) Based on Natural Photosensitizer of Butterfly Pea Flowers. *Jurnal Pijar Mipa*, *19*(3), 507–513. https://doi.org/10.29303/jpm.v19i3.6636

to prevent leakage but attain electron recombination quickly. Polymer membranes with a thickness of 0.2 mm were procured by casting knife and the phase inversion technique. The effect of PEI/DMAc polymer membrane variations on DSSC was evaluated based on open circuit voltage (V_{OC}), short circuit current density (J_{SC}), filling factor (FF), and efficiency (η). The performance of DSSC based on PEI/DMAc polymer membrane was compared to that of liquid electrolytes. Therefore, the existence of DSSC with this membrane is intended to support global energy needs, which continue to increase with the urgency of changing energy to be more environmentally friendly, which will positively impact other sectors.

Research Methods

This research is an actual experiment with a one-shot case study design. The equipment used was an automatic film applicator (TQC Sheen), magnetic stirrer (NESCO Lab MS-H280-Pro), scanning electron microscope (FEI Inspect S50), and x-ray diffraction (PANalytical X'Pert PRO).

Natural photosensitizer from dried butterfly pea flowers (BPF) made by the maceration method for 60 minutes. The liquid electrolyte (I_2) was stirred for around 30 minutes. The polymer membrane solution was derived from PEI and DMAc compositions (shown in Table 1), stirring at 60 °C for 90 minutes. The solution was cast at 30 °C within 30 minutes. The PEI/DMAc membrane was washed with distilled water. The PEI/DMAc membrane was dried for about 24 hours.

Table 1. Polymer membrane composition

Sample	Composition (%b/b)	
	PEI	DMAc
M_0	0	0
M_1	12	88
M_2	14	86
M_3	16	84
M_4	18	82
M_5	20	80

The DSSC circuit is arranged in a sandwich system (shown in Figure 1). This system uses PEI/DMAc membranes immersed in a liquid electrolyte solution for 60 minutes. The photoanode is coated in FTO glass with TiO_2 and then immersed in BPF extract for 24 hours. Meanwhile, photocathode glass is FTO glass coated with carbon.

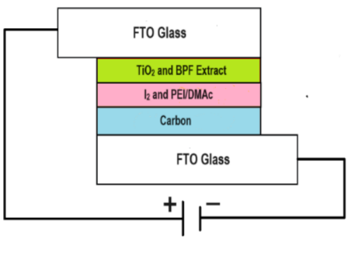

Figure 1. Sandwich system on DSSC [16]

BPF extract was characterized using a UV-Vis spectrophotometer to measure wavelength and a voltammeter to analyze the energy band gap. The DSSC circuit was measured for current and voltage values using a multimeter to determine the values of open-circuit photovoltage (V_{OC}), short-circuit current density (J_{SC}), fill factor (FF), and efficiency (η). The PEI/DMAc polymer electrolyte membrane with the best DSSC efficiency was observed using scanning electron microscopy (SEM) to determine morphology and x-ray diffraction (XRD) to analyze crystallinity.

Results and Discussion

The Wavelength of Butterfly Pea Flower Extract

The dominant color of butterfly pea flower extract (BPF) was studied using a UV-Vis spectrophotometer. Figure 2 shows two absorption peaks at 573 and 617 nm wavelengths, which qualitatively confirmed the presence of anthocyanins in the visible range of 400–800 nm. Kusumawati et al. in 2023 [17] confirmed that this wavelength indicates the dominant form of anthocyanin in BPF extract. Thuy et al. in 2021 [18] and Widyadharma et al. in 2020 [19] revealed specifically that the anthocyanin derivative compounds in BPF extract include delphinidin and cyanidin.

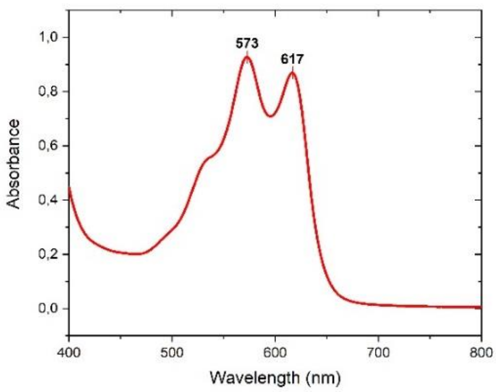

Figure 2. The UV-Vis spectrum of BPF Extract

The anthocyanin of BPF extract at 573 and 617 nm are stable towards pH, temperature, and light [20,21]. This can occur due to these compounds' antioxidant and metabolite properties [22]. Therefore, BPF extract with good stability can be promising when used as a natural photosensitizer in DSSC.

The Band Gap of Butterfly Pea Flower Extract

The influence of anthocyanins in electrochemistry is explained by Figure 3, which shows the cyclic voltammogram of the butterfly pea flower extract (BPF) with a solid copper amalgam (CuSAE) working electrode, a platinum (Pt) reference electrode, and an Ag/AgCl auxiliary electrode.

The cyclic voltammogram shows oxidation and reduction potential (Rox) (E_{red}). The HOMO and LUMO value are processed using 4.40 eV as the standard energy level of iodine electrolyte [23]. Then, the band gap is obtained from the equation:

$$\Delta E = E_{LUMO} - E_{HOMO}$$

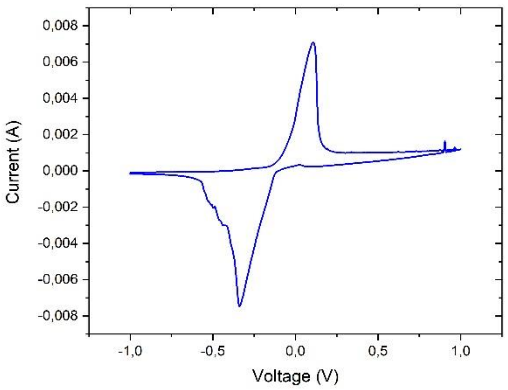

Figure 3. Cyclic voltammogram of BPF extract

Table 2 shows a comparison of electrochemical values between BPF and TiO_2. This value can explain the photoconductive properties of TiO_2, which are greatly influenced by the band gap produced by its extract. Abdulrahman et al. in 2023 [24] described that its extract can improve photoanode performance in DSSC. According to Zhou et al. in 2023 [25], the band gap relation between TiO_2 and BPF extract can improve photoelectrochemical performance.

Table 2. Electrochemical comparison between photosensitizer and photoanode

Sample	Parameter (eV)				
	E_{ox}	E_{red}	HOMO	LUMO	Band Gap
Photosensitizer BPF Extract	0.11	-0.41	-4.51	-3.99	0.52
[a]Photoanode TiO_2[a]	-3.6	-0.4	-0.8	-4.00	3.2

[a]Setiarso et al. in 2023 [23]

The HOMO of the BPF extract was lower than the TiO_2 photoanode. The LUMO of the BPF extract was slightly larger than the TiO_2 photoanode. The HOMO of the photosensitizer must be lower than the photoanode, and the LUMO of the photosensitizer must be higher than the photoanode [17]. The difference in value will facilitate optimal electron transfer [26]. Furthermore, forming a complex between BPF and TiO_2 molecules can optimize the absorption energy requirements [27]. Besides that, the band gap of the BPF extract was smaller than TiO_2. According to Pallikkara & Ramakrishnan in 2020 [28], the band gap of TiO_2 must be higher than BPF to raise optimal charge and light absorption. Furthermore, the more negligible band gap difference will make it easier for TiO_2 to absorb photons in the BPF extract because of the much smaller excitation energy, allowing greater and faster electron recombination.

A good photoanode can provide an efficient surface area for the charge of the photosensitizer, nanostructure for high light harvesting, and fast electron transport [29]. However, it is essential to note that there is a balance to be struck. Optimizing bandgap differences is just one aspect of improving DSSC efficiency. Other component factors in the DSSC must be considered to achieve the best overall performance.

Efficiency Decrease of DSSC

J-V curve is used to understand DSSC performance. The J_{SC} is normalized to the DSSC active area; thus, the curves can easily be compared from different samples [30]. The J-V curve in DSSC is based on liquid electrolytes and membrane compositions at a light intensity of 4.5×10^{-4} $mW.cm^{-2}$. The J-V curve in Figure 4 shows the membrane effect in holding liquid electrolytes. The optimal curve is obtained at M_0, which does not use a membrane. This can happen because electron recombination occurs more quickly than membrane assistance. However, a liquid electrolyte that easily leaks significantly reduces DSSC performance efficiency over a long period.

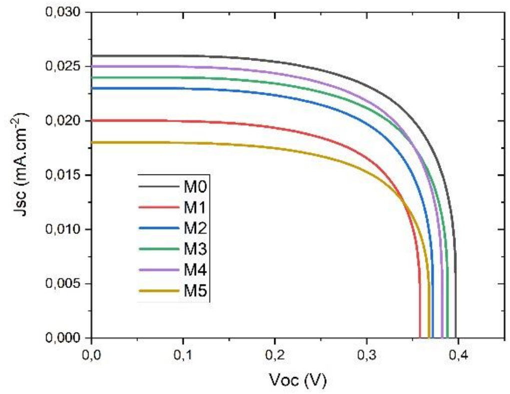

Figure 4. J-V curve in DSSC

Furthermore, photovoltaic parameters, as shown in Table 3, show the values of open circuit voltage (V_{OC}), short circuit current density (J_{SC}), filling factor (FF), and efficiency (η). This value determines the further influence of the membrane on DSSC performance efficiency. Based on the results, the use of PEI polymer membranes in DSSC has been proven to significantly maintain performance efficiency to the point of competing with M0, which only comes from liquid electrolytes. Ryzhkov et al. in 2019 [31] also found that PEI polymer membranes can increase the interface contact between DSSC electrodes, thereby maintaining their performance efficiency. Khir et al. in 2022 [32] reported that membranes could retain the efficiency performance over a long period. These studies demonstrate that its membranes can positively impact DSSC efficiency and address liquid electrolyte leakage.

V_{OC} is defined as the difference between the fermi level of the TiO_2 semiconductor and the redox level of the liquid electrolyte. This difference is due to electrons generated by photons in the TiO_2 conduction band. The transport rate of electrons produced by photons from TiO_2 to the counter electrode and then to the electrolyte and dye will be higher when the ionic conductivity of an electrolyte is high. The charge transport in large quantities and at the interface is high for liquid electrolytes [12]. Therefore, the difference between the fermi and redox levels is lower for DSSC with high-conducting electrolytes because faster charge transport causes a reduction in the number of conduction band-generated electrons [33]. When the circuit opens, the conduction band electrons recombine with ions in the electrolyte and holes in the valence band. A high recombination rate in an open circuit occurs when the charge transfer kinetics are faster [34].

Table 3. DSSC Performance Parameter

Sample	Performance Parameters			
	V_{OC} (V)	J_{SC} (mA.cm^{-2})	FF	η (%)
M_0	0.397	0.026	0.72	1.66
M_1	0.358	0.020	0.71	1.11
M_2	0.372	0.023	0.70	1.31
M_3	0.388	0.024	0.76	1.60
M_4	0.382	0.025	0.70	1.51
M_5	0.368	0.018	0.69	1.04

The fill Factor (FF) is another important parameter in determining DSSC performance efficiency. FF remained almost the same for all DSSCs in this study. This can be caused by the use of similar photoelectrodes in cells. DSSC efficiency on samples M_0 - M_5 was 1.66%, 1.11%, 1.31%, 1.60%, 1.51%, and 1.04%. These results show that DSSC based on a liquid electrolyte with PEI polymer membrane has optimal efficiency at the M_3 membrane of 1.60% and decreases at the M_4 and M_5 membranes. According to Hasan et al. in 2020 [35] and Hampu et al. in 2020 [36], this occurs because the high concentration of the polymer membrane allows the formation of narrow pores, resulting in prolonged electron recombination because the electrolyte liquid is trapped in the membrane matrix. Thus, the higher the FF, the better the efficiency of DSSC performance in converting sunlight into electrical energy. Therefore, the PEI polymer membrane reaches its optimal limit at M_3 by forming a polymer membrane structure matrix that can facilitate good ionic transport through an interconnected pore structure. However, further analysis is needed regarding the percentage reduction in efficiency over a certain period to find the best PEI polymer membrane.

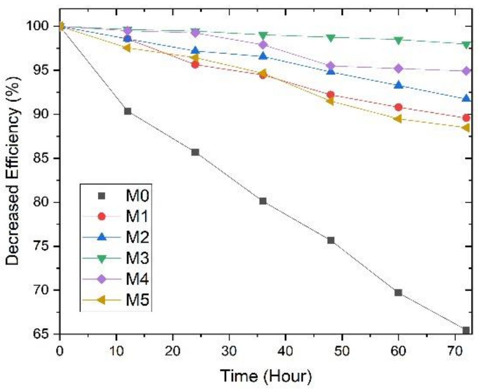

Figure 5. DSSC efficiency decreased

Figure 5 shows a graph showing that efficiency decreased over 72 hours. Sample M_0, a liquid electrolyte without a membrane, experienced the most drastic decrease in efficiency, up to 65%. This was done by Abbasi et al. in 2022 [13], who stated that the efficiency of liquid electrolytes very quickly decreases due to solvent evaporation and leakage. The M_3 membrane was proven to have stability in maintaining DSSC performance efficiency by achieving a reduction of 98% because the electrolyte liquid was retained in the membrane matrix. This gives DSSC the advantage of having a liquid electrolyte that can be used longer.

Membrane Morphology

The surface morphology of the M_3 membrane using SEM is smooth, homogeneous, dense, and porous (shown in Figure 6). According to Al-Ghafri et al. in 2019 [37], this morphology improved the quality of contact between the membrane and electrode. Kusumawati et al. (2019) [38] reported that its morphology provides good conduction properties because the empty space between the pores can provide minimal electrical resistance with maximum electric voltage and current. This can also reduce the buildup of ions due to heat or reflected light.

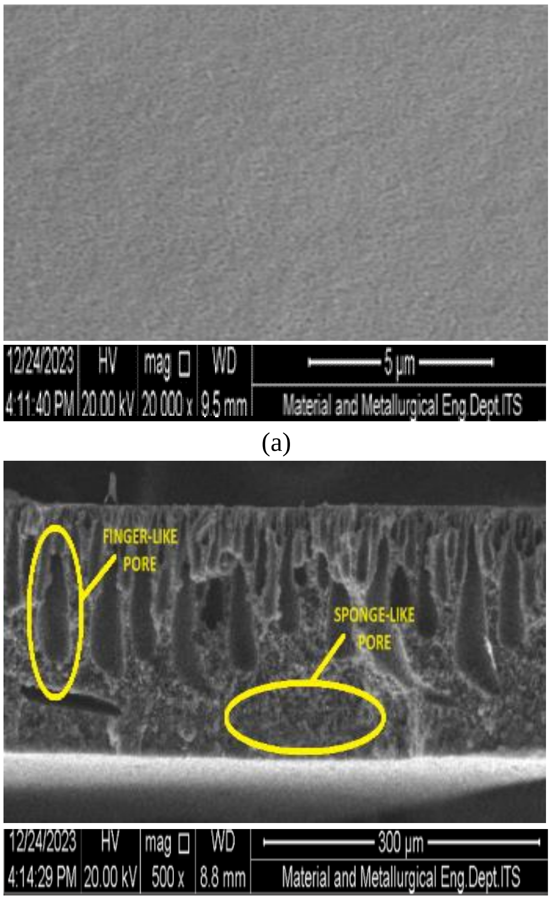

(b)

Figure 6. The M_3 membrane morphology: (a) Surface (20,000x magnification); (b) Cross-section (500x magnification)

The cross-sectional morphology of the M_3 membrane has an asymmetric structure characterized by the presence of sponge-like pores and finger-like pores. Cui et al. in 2023 [39] found the same thing: that the nodules in the cross section were parallel to the angular direction, with a transparent and dense layer near the inner surface. Wang et al. in 2024 [40] confirmed that the asymmetric structure shows the different pore sizes. Helali et al. in 2020 [41] and Duraikkannu et al. in 2021 [42] correlated the asymmetric structure due to the phase inversion method, where the top layer undergoes compaction first, supported by an expanding structure in the bottom layer.

Crystallinity Properties

Based on Figure 7, the M_3 membrane shows a broad diffraction pattern at the center position 16.25504° without intense and sharp peaks. This pattern provides a low peak distribution and impact; no significant crystals appear. Therefore, this pattern offers a membrane with an amorphous structure.

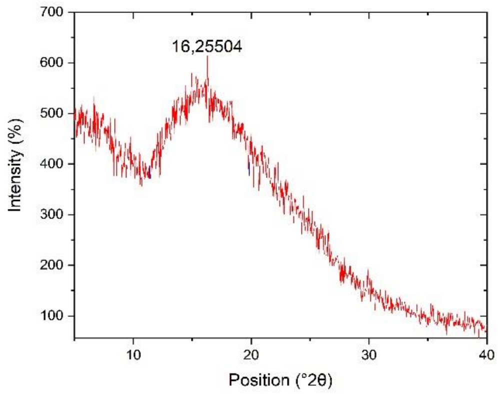

Figure 7. M_3 membrane diffractogram

The peak positions and average distance between the d-spacing of M_3 membranes are shown in Table 4. According to Bragg's law, peaks can shift to lower angles due to increasing d-spacing of a substance. Then, its membrane's amorphous structure results in a low degree of crystallinity [43]. The degree of crystallinity of a material influences the electron transfer properties of the membrane.

Table 4. Peak Value Analysis of PEI Polymer Membranes

Postion (°2θ)	FWHM (°2θ)	*d-spacing* (Å)	Degree of Crystallinity (%)
16.25504	0.0900	5.50914	12.77

The degree of crystallinity of the M_3 membrane was obtained at 12.77%. According to Nasr & Svoboda in 2023 [44] and Unger et al. in 2022 [45], its membranes have a degree of crystallinity in the range of 10-30%. The lower degree of crystallinity could impact more amorphous membranes. This is in line with Gerdroodbar et al. in 2023 [46]. The amorphous shape makes it easier for the liquid electrolyte to be retained in the membrane matrix, and the liquid electrolyte does not leak easily because of the liquid electrolyte ions in an amorphous structure located inside the helix. Apart from that, Azmar et al. 2019 [47] explain that polymer membranes with an amorphous structure can also cause high conductivity in liquid electrolytes and increase electrolyte stability by up to 42-63%. The DSSC efficiency proves this results on M_3 of 98%, which is very stable compared to M0, which fell to 65% simultaneously.

Conclusion

This research concludes that butterfly flower extract (BPF) is dominated by 573 and 617 nm wavelengths, which are part of the anthocyanin compound. The BPF extract also has a smaller band gap than the TiO_2 photoanode, making it easier for photons to be excited. Furthermore, the most stable DSSC efficiency was obtained on M_3 with an efficiency reduction percentage of 98%. The membrane has a smooth and homogeneous surface morphology, dense and porous, and a cross-sectional morphology with an asymmetric structure. In addition, the M_3 membrane has an amorphous structure with a degree of crystallinity of 12.77%. These membrane properties provide a high chance that DSSC can maintain its performance efficiency for a long. Furthermore, this research requires applicable development to fulfill its potential as a new solar panel that can be used on a massive scale.

Acknowledgments

The author is very grateful to the supervisors who have helped so that this article can be published. Thanks are also expressed to Universitas Negeri Surabaya for providing a platform for writers to develop.

References

[1] Ayuketah, Y., Gyamfi, S., Diawuo, F. A., & Dagoumas, A. S. (2023). Assessment of low-carbon energy transition policies for the energy demand sector of Cameroon. *Energy for Sustainable Development: The Journal of the International Energy Initiative*, 72, 252–264.

[2] Shirazi, M., & Fuinhas, J. A. (2023). Portfolio decisions of primary energy sources and economic complexity: The world's large energy user evidence. *Renewable Energy*, 202, 347–361.

[3] Belaïd, F., Al-Sarihi, A., & Al-Mestneer, R. (2023). Balancing climate mitigation and energy security goals amid converging global energy crises: The role of green investments. *Renewable Energy*, 205, 534–542.

[4] Suresh, S., Prabu, K. M., Arivuselvi, R., Kandasamy, M., Pugazhenthiran, N., Kumar, S. K., Jothilakshmi, R., Murugesan, K. (2023). Cow dung extract as a low-cost and natural sensitizer for zinc oxide nanoparticles photoanode based dye-sensitized solar cell: A novel initiative for waste to energy conversion. *Results in Chemistry, 6*(101060), 101060.

[5] Kalair, A., Abas, N., Saleem, M. S., Kalair, A. R., & Khan, N. (2021). Role of energy storage systems in energy transition from fossil fuels to renewables. *Energy Storage*, *3*(1).

[6] Ebhota, W. S., & Tabakov, P. Y. (2023). Influence of photovoltaic cell technologies and elevated temperature on photovoltaic system performance. *Ain Shams Engineering Journal*, 14(7), 101984.

[7] Roy, P., Ghosh, A., Barclay, F., Khare, A., & Cuce, E. (2022). Perovskite solar cells: A review of the recent advances. *Coatings*, *12*(8), 1089.

[8] Devadiga, D., Selvakumar, M., Shetty, P., & Santosh, M. S. (2021). Recent progress in dye-sensitized solar cell materials and photo-supercapacitors: A review. *Journal of Power Sources*, 493(229698), 229698.

[9] Noorasid, N. S., Arith, F., Mustafa, A. N., Azam, M. A., Mahalingam, S., Chelvanathan, P., & Amin, N. (2022). Current advancement of flexible dye

sensitized solar cell: A review. *Optik*, 254(168089), 168089.
[10] Kim, J. H., Kim, D. H., So, J. H., & Koo, H. J. (2021). Toward Eco-friendly dye-sensitized solar cells (DSSCs): Natural dyes and aqueous electrolytes. Energies, 15(1), 219.
[11] Amogne, N. Y., Ayele, D. W., & Tsigie, Y. A. (2020). Recent advances in anthocyanin dyes extracted from plants for dye sensitized solar cell. *Materials for Renewable and Sustainable Energy*, *9*(4).
[12] Kurokawa, Y., Kato, T., & Pandey, S. S. (2023). Fabrication of solid-state dye-sensitized solar cells by controlled evaporation of solvents for creation of facile charge transport pathway. *Physica Status Solidi (a)*.
[13] Abbasi, A., Xu, Y., Khezri, R., Etesami, M., Lin, C., Kheawhom, S., & Lu, Y. (2022). Advances in characteristics improvement of polymeric membranes/separators for zinc-air batteries. *Materials Today Sustainability*, *18*, 100126.
[14] Alkhouzaam, A., & Qiblawey, H. (2021). Novel polysulfone ultrafiltration membranes incorporating polydopamine functionalized graphene oxide with enhanced flux and fouling resistance. *Journal of Membrane Science*, *620*, 118900.
[15] Tan, M., He, G., Dai, Y., Wang, R., & Shi, W. (2014). Calculation on phase diagrams of polyetherimide/N,N-dimethylacetamide/H2O-BuOH casting system and their relevance to membrane performances. *Frontiers of Chemical Science and Engineering*, *8*(3), 312–319.
[16] Neetu, Maurya, I. C., Gupta, A. K., Srivastava, P., & Bahadur, L. (2017). Extensive enhancement in power conversion efficiency of dye-sensitized solar cell by using Al-doped TiO2 photoanode. Journal of Solid State Electrochemistry: Current Research and Development in Science and Technology, 21(5), 1229–1241.
[17] Kusumawati, N., Setiarso, P., Santoso, A. B., Muslim, S., A'yun, Q., & Putri, M. M. (2023). Characterization of poly(vinylidene fluoride) nanofiber-based electrolyte and its application to dye-sensitized solar cell with natural dyes. *Indonesian Journal of Chemistry*, *23*(1), 113.
[18] Thuy, N. M., Minh, V. Q., Ben, T. C., Thi Nguyen, M. T., Ha, H. T. N., & Van Tai, N. (2021). Identification of anthocyanin compounds in butterfly pea flowers (Clitoria ternatea L.) by ultra performance liquid chromatography/ultraviolet coupled to Mass spectrometry. *Molecules (Basel, Switzerland)*, *26*(15), 4539.
[19] Widyadharma, I. P. E., Soejitno, A., Jawi, M., Purwata, T. E., Suprapta, D. N., & Sudewi, A. A. R. (2020). Basic Properties of Anthocyanin for Pain Management. *Open Access Macedonian Journal of Medical Sciences*, *8*(F), 161–179.
[20] Escher, G. B., Wen, M., Zhang, L., Rosso, N. D., & Granato, D. (2020). Phenolic composition by UHPLC-Q-TOF-MS/MS and stability of anthocyanins from Clitoria ternatea L. (butterfly pea) blue petals. *Food Chemistry*, *331*(127341), 127341.
[21] Fu, X., Wu, Q., Wang, J., Chen, Y., Zhu, G., & Zhu, Z. (2021). Spectral characteristic, storage stability and antioxidant properties of anthocyanin extracts from flowers of butterfly pea (Clitoria ternatea L.). *Molecules (Basel, Switzerland)*, *26*(22), 7000.
[22] Juswardi, J., Yuliana, R., Tanzerina, N., Harmida, H., & Aminasih, N. (2023). Anthocyanin, antioxidant and metabolite content of butterfly pea flower (Clitoria ternatea L.) based on flowering phase. *Jurnal Pembelajaran dan Biologi Nukleus*, *9*(2), 349–360.
[23] Setiarso, P., Harsono, R. V., & Kusumawati, N. (2023). Fabrication of Dye Sensitized Solar Cell (DSSC) using combination of dyes extracted from Curcuma (*Curcuma xanthorrhiza*) rhizome and binahong (*Anredera cordifolia*) leaf with treatment in pH of the extraction. *Indonesian Journal of Chemistry*, *23*(4), 924.
[24] Abdulrahman, Z. H., Hachim, D. M., & Al‒Murshedi, A. S. N. (2023). A review study to manufacture each part of dye-sensitized solar cells. *1ST International Conference on Achieving the Sustainable Development Goals*.
[25] Zhou, T., Li, L., Li, J., Wang, J., Bai, J., Xia, L., Xu, Q., & Zhou, B. (2021). Electrochemically reduced TiO2 photoanode coupled with oxygen vacancy-rich carbon quantum dots for synergistically improving photoelectrochemical performance. *Chemical Engineering Journal (Lausanne, Switzerland: 1996)*, *425*(131770), 131770.
[26] Li, Y., Zhang, W., Li, X., & Xu, Y. (2021). Boosting the photoelectric conversion efficiency of DSSCs through graphene quantum dots: insights from theoretical study. *Materials Chemistry Frontiers*, *5*(15), 5814–5825.
[27] Mirzaei, M., Rasouli, A. H., & Saedi, A. (2021). HOMO-LUMO photosensitization analyses of coronene-cytosine complexes. *Main Group Chemistry*, *20*(4), 565–573.
[28] Pallikkara, A., & Ramakrishnan, K. (2021). Efficient charge collection of photoanodes and light absorption of photosensitizers: A review. *International Journal of Energy Research*, *45*(2), 1425–1448.
[29] Shittu, H. A., Bello, I. T., Kareem, M. A., Awodele, M. K., Sanusi, Y. K., & Adedokun, O. (2020). Recent developments on the photoanodes employed in dye-sensitized solar cell. *IOP Conference Series. Materials Science and Engineering*, *805*(1), 012019.
[30] Xu, Z., Wang, L., Hong, S., & Chen, G. (2021). Generalized joint shuffled scheduling decoding algorithm for the JSCC system based on protograph-LDPC codes. *IEEE Access: Practical Innovations, Open Solutions*, *9*, 128372–128380.
[31] Ryzhkov, N. V., Brezhneva, N., & Skorb, E. V. (2019). Feedback mechanisms at inorganic–polyelectrolyte interfaces for applied materials. *Surface Innovations*, *7*(3–4), 145–167.
[32] Khir, H., Pandey, A. K., Saidur, R., Ahmad, M. S., Rahim, N. A., Dewika, M., & Samykano, M. (2022). Recent advancements and challenges in flexible low temperature dye sensitised solar cells. *Sustainable*

Energy Technologies and Assessments, *53*(102745), 102745.

[33] Vargas-Barbosa, N. M., & Roling, B. (2020). Dynamic ion correlations in solid and liquid electrolytes: How do they affect charge and mass transport? *ChemElectroChem*, *7*(2), 367–385.

[34] Chen, M., Dong, H., Xue, M., Yang, C., Wang, P., Yang, Y., Zhu, H., Wu, C., Yao, Y., Luo, W., & Zou, Z. (2021). Faradaic junction and isoenergetic charge transfer mechanism on semiconductor/semiconductor interfaces. *Nature Communications*, *12*(1).

[35] Hasan, M. M., Islam, M. D., & Rashid, T. U. (2020). Biopolymer-based electrolytes for dye-sensitized solar cells: A critical review. *Energy & Fuels: An American Chemical Society Journal*, *34*(12), 15634–15671.

[36] Hampu, N., Werber, J. R., Chan, W. Y., Feinberg, E. C., & Hillmyer, M. A. (2020). Next-generation ultrafiltration membranes enabled by block polymers. *ACS Nano*, *14*(12), 16446–16471.

[37] Al-Ghafri, B., Lau, W.-J., Al-Abri, M., Goh, P.-S., & Ismail, A. F. (2019). Titanium dioxide-modified polyetherimide nanofiber membrane for water treatment. *Journal of Water Process Engineering*, *32*(100970), 100970.

[38] Kusumawati, N., Setiarso, P., Budi Santoso, A., Chendra Wibawa, S., & Muslim, S. (2019). The development of pvdf/Pei blended membrane: Effect of stirring time on membrane characteristics and performance. *Rasayan Journal of Chemistry*, *12*(02), 975–986.

[39] Cui, Y., Li, G., Wu, H., Pang, S., Zhuang, Y., Si, Z., Zhang, X., & Qin, P. (2023). Preparation and characterization of asymmetric Kapton membranes for gas separation. *Reactive & Functional Polymers*, *191*(105667), 105667.

[40] Wang, Z., Zeng, Y., Shen, Y., Tan, Q., Sun, J., Teng, J., & Lin, H. (2024). Innovative integration of porous materials and membranes: Achieving optimized pore orientation for enhanced performance. *Journal of Membrane Science*, *689*(122158), 122158.

[41] Helali, N., Rastgar, M., Farhad Ismail, M., & Sadrzadeh, M. (2020). Development of underwater superoleophobic polyamide-imide (PAI) microfiltration membranes for oil/water emulsion separation. *Separation and Purification Technology*, *238*(116451), 116451.

[42] Duraikkannu, S. L., Castro-Muñoz, R., & Figoli, A. (2021). A review on phase-inversion technique-based polymer microsphere fabrication. *Colloids and Interface Science Communications*, *40*(100329), 100329.

[43] Dolabella, S., Borzì, A., Dommann, A., & Neels, A. (2022). Lattice strain and defects analysis in nanostructured semiconductor materials and devices by high-resolution X-ray diffraction: Theoretical and practical aspects. *Small Methods*, *6*(2).

[44] Nasr, A., & Svoboda, P. (2023). Influence of fusion temperature on nonisothermal crystallization kinetics of polyamide 6. *Polymers*, *15*(8), 1952.

[45] Unger, L., Dechet, M. A., Fischer, S., Schmidt, J., & Bück, A. (2022). Semi-crystalline polyetherimide microparticles via liquid-liquid phase separation and precipitation. *Macromolecular Materials and Engineering*, *307*(4).

[46] Gerdroodbar, A. E., Alihemmati, H., Safavi-Mirmahaleh, S.-A., Golshan, M., Damircheli, R., Eliseeva, S. N., & Salami-Kalajahi, M. (2023). A review on ion transport pathways and coordination chemistry between ions and electrolytes in energy storage devices. *Journal of Energy Storage*, *74*(109311), 109311.

[47] Azmar, A., Subban, R. H. Y., & Winie, T. (2019). Improved long-term stability of dye-sensitized solar cell employing PMA/PVAc based gel polymer electrolyte. *Optical Materials*, *96*(109349), 109349.